Millisecond Production of Hydrogen from Alternative, High Hydrogen Density Fuels in a Cocurrent Multifunctional Microreactor

ARTICLE *in* INDUSTRIAL & ENGINEERING CHEMISTRY RESEARCH · FEBRUARY 2009

Impact Factor: 2.59 · DOI: 10.1021/ie800392z

3 AUTHORS:

Niket S. Kaisare
Indian Institute of Technology Madras
46 PUBLICATIONS **553** CITATIONS
SEE PROFILE

Georgios D. Stefanidis
University of Leuven
57 PUBLICATIONS **532** CITATIONS
SEE PROFILE

Dionisios G Vlachos
University of Delaware
410 PUBLICATIONS **9,474** CITATIONS
SEE PROFILE

Article

Millisecond Production of Hydrogen from Alternative, High Hydrogen Density Fuels in a Cocurrent Multifunctional Microreactor

Niket S. Kaisare, Georgios D. Stefanidis, and Dionisios G. Vlachos

Ind. Eng. Chem. Res., **2009**, 48 (4), 1749-1760• DOI: 10.1021/ie800392z • Publication Date (Web): 12 January 2009

Millisecond Production of Hydrogen from Alternative, High Hydrogen Density Fuels in a Cocurrent Multifunctional Microreactor

Niket S. Kaisare,[¶] Georgios D. Stefanidis, and Dionisios G. Vlachos*

Department of Chemical Engineering and Center for Catalytic Science and Technology, University of Delaware, 150 Academy Street, Newark, Delaware 19716

A pseudo-2-dimensional model is used for modeling a multifunctional microreactor for hydrogen generation by coupling catalytic ammonia decomposition on ruthenium with catalytic propane combustion on platinum. The two reactions are carried out in adjacent parallel plate channels in a cocurrent flow mode. Operating lines defining the attainable region are computed. The high temperatures and fast heat transfer ensure that both reactions go to completion in as low as submillisecond contact times and enable compact hydrogen production for portable and distributed power generation. The ammonia decomposition reaction tends to be limited by the intrinsic rate of reaction, whereas catalytic combustion is also affected by mass and heat diffusion. We have found that moderate and high conductivity materials are preferable because they support a rather wide attainable region. We show that one such device could enable variable hydrogen supply for variable power needs. A simple operating strategy to dial in the desirable power is proposed, which ensures high thermal efficiency (∼75% once-through efficiency of the integrated device and ∼85% reformer efficiency, both without any heat recuperation), wall isothermicity, and high conversions.

Introduction

Realizing a hydrogen economy depends on developing efficient means for storing and transporting hydrogen.[1] Owing to its low volumetric energy density (10.7 MJ/standard m^3), low boiling point (20 K), and extremely reactive nature, storage of liquefied or pressurized hydrogen for portable or decentralized power generation applications is economically and logistically challenging.[2,3] Therefore, hydrogen storage in the form of hydrocarbons, alcohols, or ammonia—which have a higher volumetric energy density and are more readily liquefiable or compressible—followed by generation in an onboard reformer, is considered as a practical alternative. Ammonia is one of the highest hydrogen density carriers (on a mass based) and has the additional advantage, over hydrocarbons and alcohols, of representing a CO-free hydrogen source.[4] This is important because of the low CO tolerance of PEM fuel cells, eliminating the need for downstream water-gas shift and preferential oxidation reactors [5,6] or separation units. Despite these advantages over hydrocarbon fuels, stringent statutory requirements on ammonia emissions (owing to its toxicity and fuel cell lifetime) require complete ammonia conversion, which is addressed in this paper. Still, downstream strippers may be required to meet the emission norms and ensure ammonia-free supply of hydrogen.

Ammonia decomposition $2NH_3 \rightarrow N_2 + 3H_2 + 91.8$ kJ/mol is a mildly endothermic reaction. Complete conversion to hydrogen can be achieved catalytically at high temperatures and atmospheric pressure on noble metal catalysts, typically Ruthenium (Ru).[4,7,8] The energy required for this reaction can be provided via combustion of fuels. A comprehensive review of the state of the art and emerging trends for hydrogen generation at various scales, ranging from industrial production to portable microreformers, was given in ref 9. The authors reported a growing trend toward using "multifunctional reactors," a concept popularized two decades ago,[10,11] where exothermic combustion, endothermic reactions, and heat transfer are integrated in a single device. While the principles are fairly well understood for larger scale devices, little is known about the design of small scale ones.

Thermal coupling between endothermic and exothermic reactions can be achieved in various ways, which have been reviewed extensively.[12,13] One entails the direct physical coupling of two reactions in the same catalytic bed/channel, such as autothermal reforming[14] or partial oxidation.[15] An alternative means is to spatially separate the endothermic and exothermic reactions on either side of a heat exchanger.[16−18] A review of spatially coupled multifunctional reactors for hydrogen production is provided in ref 17. A third strategy is to achieve temporal coupling by utilizing the thermal capacity of the reactor body to store the heat generated in one cycle and release it in the next cycle.[19,20] Likewise, the heat regenerative capability of the reactor body can be utilized to maintain autothermal operation of mildly exothermic oxidation processes in a reverse-flow reactor.[21−24] Several different dynamic operation strategies that employ spatially coupled reactors[25] or multiple reactors in series[26] have also been analyzed.

The conventional hydrogen production route is too bulky (residence time of a few seconds). A key requirement for onboard and more generally distributed hydrogen generation is system compactness. Recently, we investigated coupling ammonia decomposition on Ru-supported catalyst and homogeneous propane combustion in countercurrent[17] and cocurrent[18] microreactors. Similar to large-scale reactors, the spatial separation of reaction zones along the axis in the endothermic and exothermic channels in the counter-current operation resulted in hot spot formation and large temperature gradients. As a result, the cocurrent configuration was the most favored operation mode from a materials stability standpoint. In our previous work, we demonstrated that it is feasible to supply heat to the endothermic reaction via homogeneous combustion at millisecond contact times but the operating region is too narrow for practical purposes. In other words, the large-scale analogue of flames heating a reformer does not scale down well.[27,28]

* To whom correspondence should be addressed. E-mail: vlachos@udel.edu. Tel.: (302) 831-2830. Fax: (302) 831-1048.

[¶] Current address: Department of Chemical Engineering, Indian Institute of Technology—Madras, Chennai 600-036, India.

10.1021/ie800392z CCC: $40.75
Published on Web 01/12/2009

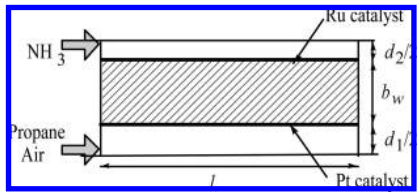

Figure 1. Schematic of the parallel plate catalytic reactor with alternating catalytic combustion and ammonia decomposition channels. Pt and Ru catalysts are coated on the opposite walls of the parallel plate. The dash-dotted lines are the axes of symmetry. The side walls are insulated and the entire reactor is adiabatic.

In this paper, we extend the idea proposed in our previous work by using catalytic combustion of propane on Pt/Al_2O_3 to provide the heat required for ammonia decomposition on Ru/Al_2O_3 catalyst. The advantages of catalytic combustion over homogeneous combustion are the lower operating temperatures and, as we show in this paper, a larger range of conditions for stable operation. Engineering maps that delineate the preferred operating region with respect to the flow rates of combustion and ammonia streams for stable and efficient operation are developed and the role of wall thermal conductivity is investigated. Qualitative comparison with the homogeneous combustion case is also presented. Finally, the effect of these parameters on device efficiency and total power output is analyzed. A simple strategy for dialing in a specific power output is proposed.

Mathematical Model

Figure 1 shows a schematic of the computational domain of a parallel plate microreactor with alternating propane/air combustion and ammonia decomposition channels. The adjacent walls of the parallel plates are coated with Pt catalyst (combustion channel) and Ru catalyst (ammonia decomposition channel). The use of different catalysts and fuels renders the spatially coupled multifunctional reactor strategy a natural one. The plates separating the two channels are 5 cm long and 750 μm thick. The gap sizes of the combustion and the ammonia channels are 300 and 200 μm, respectively. Owing to the symmetry of the device, only two half-channels and one separating wall are modeled.

The reactor is modeled using a *pseudo-2D model* (also called 1D heterogeneous model), which involves conservation equations in the axial direction (of each channel and the separating wall) and a lumped parameter description of transverse heat and mass transfer in each channel (between the bulk gas and the wall). The main feature of the pseudo-2D model is that the transverse heat and mass transfer correlations were chosen based on 2D computational fluid dynamics (CFD) models. Detailed discussion of the model was provided in our previous paper;[29] the resulting conservation equations are summarized in Table 1.

The reactor width in the third dimension is assumed to be 1 cm whenever reporting flow rates in SLPM (standard liters per minute) and the power generated. Table 2 lists the relevant operating parameters.

The thermodynamic and transport properties are obtained from the CHEMKIN database.[30,31] Transverse heat and mass transfer coefficients are computed assuming constant values of Nusselt ($Nu = 4.0$) and Sherwood ($Sh = 3.8$) numbers as was found in ref 32. The transverse transport rates vary along the reactor axis on the basis of the local temperature and composition, according to eq T-6 shown in Table 1. The axial diffusion coefficient in the two channels was kept constant (to improve numerical stability) at $D_{avg}^{exo} = 1.99$ cm^2/s and $D_{avg}^{endo} = 3.4$ cm^2/s. The axial diffusivity for the combustion channel is the mass fraction weighted diffusivity at 1123 K for a propane/air mixture with an equivalence ratio of 0.85; that for the ammonia channel is similarly computed at 1123 K for 25% ammonia conversion. This assumption is reasonable because the axial Peclet number is at least 150 (even for our slower flows), that is, convection dominates, and any diffusion approximation is of secondary importance. For the same reason, Dirichlet boundary conditions are used at the inlet.

The mass and energy conservation equations are solved using the method of lines. A finite difference scheme is employed to discretize the differential equation in 500 equidistant axial nodes. The resulting differential algebraic equations (DAEs) are solved using the DASPK package[33] employing a numerically computed banded Jacobian. The transient model is run for a sufficiently long time ensuring that steady state is attained.

Table 1. Model Equations and Boundary Conditions

Governing Equations for the Two Channels

continuity:

$$-\frac{\rho}{T_g}\frac{\partial T_g}{\partial t} - \sum_k \left[\frac{\rho \bar{M}}{M_k}\frac{\partial Y_k}{\partial t}\right] + \frac{\partial(\rho u)}{\partial x} = 0 \qquad \text{(T-1)}$$

species balance equations:

$$\frac{\partial Y_k}{\partial t} + \frac{\rho u}{\rho}\frac{\partial Y_k}{\partial x} = D_{avg}\frac{\partial^2 Y_k}{\partial x^2} - \hat{a}_g k_{mt,k}(Y_k - Y_{ks}) \qquad \text{(T-2)}$$

$$0 = \eta M_k \sum_j \nu_{kj} r_{cat,j} + \rho k_{mt,k}(Y_k - Y_{ks}) \qquad \text{(T-3)}$$

energy balance equations:

$$\rho \bar{c}_p \frac{\partial T_g}{\partial t} + \rho u \bar{c}_p \frac{\partial T_g}{\partial x} = \frac{\partial}{\partial x}\left(k_g \frac{\partial T_g}{\partial x}\right) - \hat{a}_g h_g (T_g - T_s) \qquad \text{(T-4)}$$

Governing Equation for the Wall

$$\rho_s c_s \frac{\partial T_s}{\partial t} = k_s \frac{\partial^2 T_s}{\partial x^2} + \eta \hat{a}_s \sum_j \Delta H_j r_{cat,j}^{exo} + \eta \hat{a}_s \sum_j \Delta H_j r_{cat,j}^{endo} + h_g^{exo} \hat{a}_s (T_g^{exo} - T_s) + h_g^{endo} \hat{a}_s (T_g^{endo} - T_s) \qquad \text{(T-5)}$$

Transverse Heat and Mass Transport

$$h_g = Nu\frac{k_g}{d}, \quad \text{and} \quad k_{mt,k} = Sh\frac{D_k}{d} \qquad \text{(T-6)}$$

Boundary conditions

At inlet, $x = 0$:

$$\begin{cases} u^i = u_0^i, & Y_k^i = Y_{k0}^i, \quad T_g^i = T_{g0}^i \\ & \dfrac{\partial T_s}{\partial x} = 0 \end{cases} \qquad \text{(T-7)}$$

At outlet, $x = l$:

$$\frac{\partial Y_k^i}{\partial x} = \frac{\partial T_k^i}{\partial x} = \frac{\partial T_s}{\partial x} = 0 \qquad \text{where } i = \text{exo; endo} \qquad \text{(T-8)}$$

Table 2. Operating Conditions and Model Parameters Used in Simulations

length	l	5 cm
plate thickness	b_w	750 μm
wall conductivity	k_s	3, 15, 75, 300 W/m/K
combustion channel		
gap width	d_1	300 μm
equivalence ratio	ϕ	0.85[a]
inlet velocity	u_0	varies
inlet temperature	T_{in}	300 K
ammonia channel		
gap width	d_2	200 μm
NH_3 composition	Y_0	99.9%[b]
inlet velocity	u_0	varies
inlet temperature	T_{in}	300 K

[a] Equivalence ratio of 0.85 corresponds to 5.17% propane and 22.1% oxygen (rest, nitrogen) by weight. [b] The ammonia feed contains 0.05% N_2 and H_2 by weight.

Table 3. Kinetic Rate Parameters for Propane Combustion Used in Equation 4[a]

reaction	A_0 (s^{-1}) or s (—)	β	E_{act} (kcal/mol)
adsorption: $C_3H_8 + 2^* \rightarrow C_3H_7^* + H^*$	0.06	0.154	4.0
adsorption: $O_2 + 2^* \rightarrow 2O^*$	0.0542	0.766	0.0
desorption: $2O^* \rightarrow O_2 + 2^*$	8.41×10^{12}	−0.796	$E_{O2}^{des} = 52.8 - 2.3(T/300) - 32.0\theta_{O^*}$

[a] The activation energy for oxygen desorption depends on the oxygen surface coverage (θ_{O^*}) and the temperature. The catalyst surface site density is $\Gamma = 2.5 \times 10^{-9}$ mol/cm^2. $T_{ref} = 300$ K.

Reaction Kinetics. Reduced-order rate expressions for catalytic propane combustion on Pt[34] and ammonia decomposition on *Ru*,[8] obtained via a posteriori reduction of microkinetic models[35] are used in this work. The model reduction procedure and the use of the resulting rate expressions in CFD and pseudo-2D models was discussed in detail elsewhere.[29,36]

The rate of propane combustion

$$C_3H_8 + 5O_2 \rightarrow 3CO_2 + 4H_2O$$

(in turnover frequency units, i.e., molecules reacting per catalyst site per second) is given by

$$\sigma_{C_3H_8} = \frac{k_{C_3H_8}^{ads} X_{C_3H_8}}{\left(1 + \sqrt{\frac{k_{O_2}^{ads} X_{O_2}}{k_{O_2}^{des}}}\right)^2} \quad (1)$$

In the above expression, the species adsorption rate constant is

$$k_k^{ads} = \frac{sP_{tot}}{\Gamma}\sqrt{\frac{1}{2\pi RTM_k}}\left(\frac{T}{T_{ref}}\right)^{\beta_k^{ads}} \exp\left(\frac{-E_k^{ads}}{RT}\right) \quad (2)$$

where P_{tot} is the total pressure. The desorption rate constant is

$$k_k^{des} = A_0\left(\frac{T}{T_{ref}}\right)^{\beta_k^{des}} \exp\left(\frac{-E_k^{des}}{RT}\right) \quad (3)$$

The kinetic rate constants are provided in Table 3. Throughout this paper, $T_{ref} = 300$ K. Activation energies required in computation of the reaction rate, according to eq 1, depend on the oxygen surface coverage. The oxygen coverage is a function of temperature and oxygen mole fraction and is obtained (at each axial location) by solving the following nonlinear equation

$$\theta_{O^*} = 1 - \frac{1}{\left(1 + \sqrt{\frac{k_{O_2}^{ads} X_{O_2}}{k_{O_2}^{des}}}\right)} \quad (4)$$

The rate expression for propane combustion was independently validated against experimental results.[34] We also showed that the pseudo-2D model employing this kinetic expression reproduces the experimentally observed trends in a stand-alone catalytic microburner.[29,36]

Likewise, the rate of ammonia decomposition on Ru

$$2NH_3 \rightarrow N_2 + 3H_2$$

(in turnover frequency units) is

$$\sigma_{NH_3} = \frac{-2k_{N_2}^{des}(\omega^2 - K_{N_2}X_{N_2})}{(1 + K_{NH_3}X_{NH_3} + \sqrt{K_{H_2}X_{H_2}} + \omega)^2} \quad (5)$$

with

$$\omega = \sqrt{K_{N_2}X_{N_2} + K_{rxn}\frac{K_{NH_3}X_{NH_3}}{\sqrt{K_{H_2}X_{H_2}}}} \quad (6)$$

The kinetic rate parameters are given in Table 4. The development of kinetic rate expression and experimental validation was presented in our earlier work.[8] The equilibrium constants for adsorption of the three species and net surface reaction can be, respectively, obtained from

$$K_X = A_0\left(\frac{P_{tot}}{P_{ref}}\right)\exp\left(\frac{-\Delta H}{RT}\right) \quad \text{and} \quad K_{rxn} = A_0\exp\left(\frac{-E_{net}}{RT}\right) \quad (7)$$

where the reference pressure is $P_{ref} = 1.013 \times 10^5$ Pa. The desorption rate constant, $k_{N_2}^{des}$, is obtained using eq 3. The use of accurate reduced-order rate expressions is another distinguishing feature of our modeling approach for design of the multifunctional microreactor.

Role of Fuel and Ammonia Flow Rates. Figure 2 shows operational characteristics for three combinations of flow rates of propane/air and ammonia streams of the multifunctional microdevice. Flow occurs from left to right. Axial temperature profiles in the two channels and the wall are shown in the top panels, whereas reaction rates and conversion are plotted in the bottom panels. Note the logarithmic scale of the abscissa. As in stand-alone catalytic microburners,[29] the combustion channel can be divided into a combined preheating/combustion zone (shaded region in the top panels) and a postcombustion zone along the longitudinal axis. Unlike the homogeneous combustion case,[18] where a separate preheating zone exists upstream of the "flame" (i.e., a clearly distinct combustion zone), substantial catalytic combustion takes places in the preheating zone as well. Heat transfer takes place from the hot walls to the bulk gas owing to axial heat recirculation ("preheating") along the wall and reaction heat release ("combustion"). The reaction zone in the ammonia channel is indicated with hatched lines. Figure 2 indicates that in addition to providing high catalytic surface area (in a washcoat or a mesoporous layer), the wall is responsible for preheating the propane/air mixture to its ignition temperature as well as for heat transfer from the exothermic to the endothermic reaction.

Table 4. Parameters for Computing the Ammonia Decomposition Rate in Equation 5[a]

reaction	A_0	E_a or ΔH (kcal/mol)
K_{H_2} (H_2 adsorption/desorption)	$(5.44 \times 10^{-3})/(RT)^{1/2}$	−21.8
K_{N_2} (N_2 adsorption/desorption)	$(1.45 \times 10^{-3})/(RT)^{1/2}$	−23.1
K_{NH_3}(NH_3 adsorption/desorption)	$(1.87 \times 10^{-3})/(RT)^{1/2}$	−18.2
K_{rxn} (net surface reaction)	5×10^{-3}	−13.8
$k_{N_2}^{des}$ (N_2 desorption)	1×10^{13}	37.2

[a] Activation energies are computed at N* coverage $\theta_{N^*} = 0.3$. The catalyst surface site density is $\Gamma = 1.66 \times 10^{-9}$ mol/cm^2.

The Biot number for both channels, which is the ratio of wall−channel convective heat flux to the conductive heat flux across the wall, is low. Thus, even in the case of nonconducting walls (3 W/m/K), the heat transfer from the exothermic channel wall to the gas of the endothermic channel is limited from the heat transfer in the fluid stream. Heat transfer across the (thin) wall is much faster than the intrinsic reaction time scale. Consequently, the 1D nature of wall energy balance, which neglects transverse wall gradients, is a valid approximation since low wall thickness ensures fast heat transfer between exothermic and endothermic channels (this finding has been validated several times in our previous 2D CFD studies).

Column A represents the nominal operating condition, with inlet velocities in the combustion and ammonia channels being 6.1 and 0.92 m/s, respectively. These correspond to 1.0 SLPM flow rate of the combustible mixture and 0.1 SLPM flow rate of ammonia for a 1 cm wide microdevice (in the third dimension). For these conditions, the Reynolds number in the two channels is 115 and 20, respectively. The high combustible flow rate compared to the ammonia flow rate results in high wall temperatures (in excess of 1500 K), which are undesirable because of materials stability issues (e.g., catalyst sintering and evaporation, mechanical failure of walls). The net reaction rates are high, and complete conversion of propane and ammonia at short contact times is observed. The average contact times for these conditions in the combustion and the ammonia channels are 1.5 and 4.8 ms, respectively. These values have been computed considering an average velocity at a temperature of 1500 K. The contact times required for complete conversion (computed using the equivalent length required for 99.9% conversion shown in the lower panel of Figure 2A or by summing up the local residence times in each reactor differential up to 99.9% conversion) are in the *submillisecond range*: 0.6 and 0.5 ms, respectively.

As the ammonia flow rate is increased, at a constant propane/air flow rate (column B), reactor temperatures drop due to an increase in the heat consumed by the endothermic ammonia decomposition reaction. The lower wall temperatures and the higher NH_3 flow rate result in more extended reaction zones in both channels; the effect is more pronounced on the ammonia decomposition zone, whereas the expansion of the combustion zone is only marginal. There is also a greater overlap between the combustion and ammonia decomposition zones and the axial thermal gradients in the wall are reduced. These simulations illustrate that the flow rates of the two streams must properly be balanced to moderate the device temperature (see also below).

Column C shows results at a lower flow rate of the combustion mixture and the same ammonia flow rate as in column A. As expected, the wall temperature decreases due to lower heat generation. As the ammonia decomposition is kinetically controlled (as we show next), a longer reactor length is required for completion of the reaction because of the lower wall temperatures. It is interesting to note, however, that the combustion zone moves upstream. This behavior is similar to the one observed in a standalone catalytic microburner, where the location of the reaction zone was primarily influenced by the combustible streamflow rate.[29]

To explore transport limitations, transverse Damköhler number profiles are plotted in Figure 3 for both channels for these three cases. The Damköhler number (Da) is a ratio of transverse diffusion and reaction time scales, $Da = \tau_{diffusion}/\tau_{reaction}$, computed as follows:

$$\tau_{diffusion} = \frac{d^2}{4D} \tag{8}$$

$$\tau_{reaction} = \frac{C_{g,k}}{r_{cat}(\bar{T}, Y_{gk})\cdot\hat{a}_g} \tag{9}$$

A locally computed species mass fraction weighted average diffusivity D is used in the denominator of eq 8 and a weighted average temperature $\bar{T}$, calculated as in Kaisare et al.,[29] is used in eq 9. The Damköhler number varies moderately with position and settles to an asymptote after the initial 5% of the reactor length. The transport rates in the ammonia channel are higher owing to the higher diffusivity of ammonia and the smaller gap size. This fact, in conjunction with the slower intrinsic ammonia decomposition kinetics, renders the process kinetically controlled. In contrast, transport plays a much greater role in the combustion channel owing to a lower average diffusivity and a faster intrinsic reaction rate. Note that the net reaction rate (and not the intrinsic reaction rate) of ammonia decomposition is higher than that of propane combustion in Figure 2. At higher temperatures, that is, when the ratio of propane/air and ammonia flow rates is increased, reactions tend to be more diffusion limited.

In addition to the transverse mass diffusion, the operation of the combustion channel is also governed from transverse heat transfer responsible for preheating the incoming fuel/air mixture. Figure 2 implicitly provides information on heat transfer in the two channels. Significant transverse temperature gradients exist between the wall (symbols) and the bulk gas (solid lines) in the combustion channel for a major section of the shaded region. In contrast, the corresponding transverse gradients as well as the axial gradients in the bulk gas are lower in the ammonia channel. This difference results from the enhanced transverse conductive heat flux from the hot wall to the bulk (due to the narrower gap size) and the lower axial convective heat flux removed from the upstream cold reactant mixture (due to a lower ammonia inlet velocity).

In conclusion, the ammonia decomposition is kinetics limited, whereas kinetics, heat, and mass transfer are all important for propane combustion. The reaction rate and the length for complete conversion of ammonia decomposition are affected from the feed rates of the combustible and ammonia streams: an increase in the combustible feed flow rate (or a decrease in the ammonia feed flow rate) causes the reaction zone in the ammonia channel to move upstream. The higher the overlap of the combustion and ammonia decomposition zones, the lower and more uniform the wall temperature profile becomes, which is desirable for the catalyst and the mechanical stability of the wall. As reported for stand-alone catalytic microburners,[29] propane breakthrough occurs for fuel channel residence times (based on inlet conditions) of less than 3 ms. Given the higher residence times herein, propane breakthrough does not occur.

Role of Wall Thermal Conductivity. In recent work, we have demonstrated that the wall thermal conductivity has a

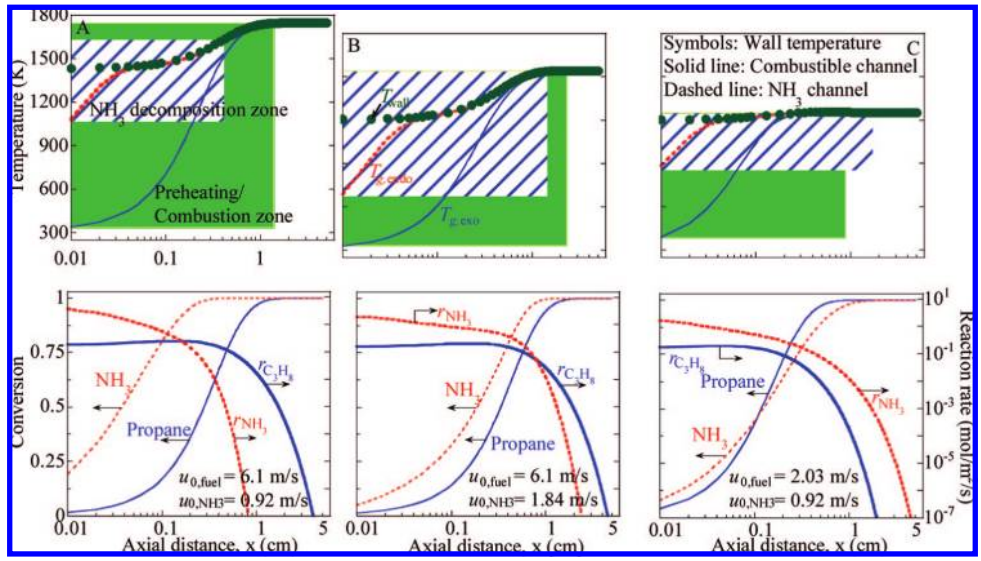

Figure 2. Effect of inlet flow rates of the combustion and the ammonia decomposition streams on axial profiles of temperature (top panels) and propane and ammonia conversion (bottom panels) for a wall thermal conductivity of $k_s = 15$ W/m/K. Reaction rates are plotted as thick lines (bottom panels). In the top panels, the shaded region demarcates the preheating/combustion zone and the hatched region the ammonia decomposition zone.

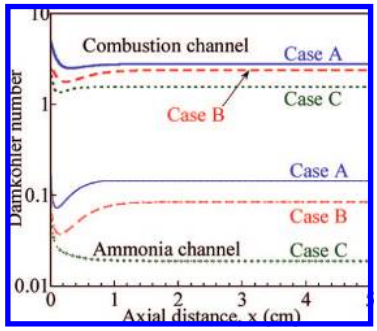

Figure 3. Axial variation of the Damköhler number for the three conditions shown in Figure 2. Ammonia decomposition tends to be reaction-limited, especially at lower temperatures (i.e., at lower combustible or higher ammonia flow rates). Diffusion and reaction rates in the combustion channel are comparable.

profound impact on the operation region of coupled microdevices employing homogeneous propane combustion.[17,18] Heat recirculation through the walls is critical for preheating the fuel/air mixture to its ignition point, and highly conducting walls were overall preferable. The effect of wall thermal conductivity on the attainable regime of stand-alone catalytic microburners was found to be weaker than their homogeneous counterparts.[29] It appears then that the effect of wall conductivity on attainable regions depends on the degree of device integration and the mode of combustion (gas vs catalytic). We explore this issue when both channels are catalytic.

In these multifunctional devices, important operating lines include (1) self-sustained device operation, (2) materials stability, and (3) reactant breakthrough. The latter two requirements are often conflicting because lower wall temperatures, although preferable for materials stability, could lead to incomplete conversion. Like our previous work, a maximum wall temperature of 1500 K is selected as a reasonable, albeit arbitrary, limit for stability of catalyst and reactor structural material (hereafter termed as materials stability limit). Since complete propane conversion is observed for the entire range of operating conditions used here, the 99% ammonia conversion value is selected to demarcate the NH_3 breakthrough line.

Figure 4a shows the maximum wall temperature vs inlet velocity of the combustion stream at a constant ammonia inlet

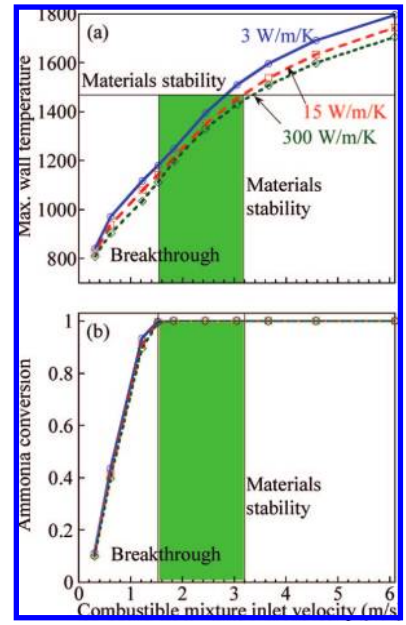

Figure 4. Effect of the combustion stream inlet velocity on (a) maximum wall temperature and (b) ammonia conversion at a constant ammonia inlet velocity 0.92 m/s for various wall thermal conductivities. The symbols denote simulation points and the lines just connect the points. The left, vertical lines denote the ammonia breakthrough limit, the horizontal line denotes the upper temperature due to the materials stability limit, the right; vertical lines the maximum velocity due to the materials stability limit, and the shaded region represents the operating region that satisfies both of these conditions for $k_s = 15$ W/m/K.

velocity. The horizontal line represents the maximum temperature due to the materials stability limit; the left, vertical lines in both panels represent the ammonia breakthrough limit; and the right, vertical lines represent the maximum propane flow rate to prevent overheating. The shaded region demarcates the operating region that satisfies both of these criteria for a wall conductivity of $k_s = 15$ W/m/K. The maximum wall temperatures are highest for the lowest wall conductivity; as the wall conductivity increases, the axial heat dissipation from the reaction zone increases causing a decrease in the maximum wall temperature. This holds across the range of combustible streamflow rates studied. Figure 4b shows that the ammonia

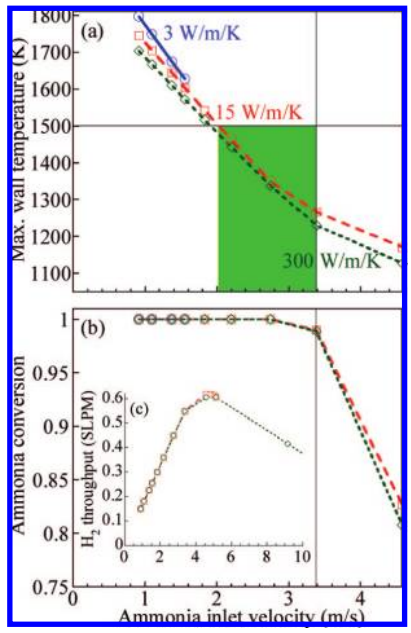

Figure 5. Effect of ammonia inlet velocity on (a) maximum wall temperature, (b) ammonia conversion, and (c) hydrogen throughput at a constant combustion stream inlet velocity of 6.1 m/s for various wall thermal conductivities. In panel c, a more expanded range of flow velocities is used to clearly show the maximum. The vertical line denotes the ammonia breakthrough limit, the horizontal line denotes the maximum temperature due to the materials stability limit; and the shaded region represents the operating region that satisfies both of these conditions for a wall conductivity of $k_s = 15$ W/m/K.

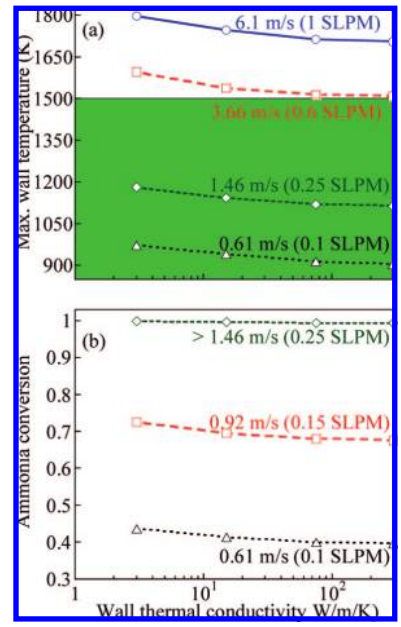

Figure 6. Effect of wall thermal conductivity on (a) maximum wall temperature and (b) ammonia conversion for an inlet ammonia velocity of 0.92 m/s and various combustible streamflow rates indicated. The shaded region in panel a represents the operating region based on the materials stability criterion. Complete conversion of ammonia is observed for a propane/air inlet velocity higher than 1.46 m/s.

conversion depends mainly on the inlet flow rates; the dependence on the wall conductivity is weak (in the incomplete conversion regime, the ammonia conversion for 300 W/m/K differs from that at 3 W/m/K by less than 10%) and cannot be easily discerned in the scale of this graph. In the incomplete conversion range, the less conductive walls give rise to higher conversions due to higher temperatures and thus faster overall kinetics.

From a practical standpoint, Figure 4 indicates that at a fixed ammonia flow rate, the combustible flow rate should be sufficiently high to supply the necessary heat and ensure complete conversion of the endothermic reaction and maximum flow rate of hydrogen (achieved upon full ammonia conversion) but not much higher (to keep temperatures low). This operating point coincides with the breakthrough line. The operating region between the materials stability limit and the breakthrough limit is narrower for insulating walls ($k_s = 3$ W/m/K), primarily due to the materials stability limit and is moderately extended for more conducting walls. Highly conducting walls allow a slightly wider range of fuel flow rates.

Similar trends are observed in Figure 5, wherein the maximum wall temperature and ammonia conversion are plotted as a function of the inlet ammonia velocity at a constant combustion stream velocity. The preferred operating region for $k_s = 15$ W/m/K is indicated by the shaded region in the top panel. A fairly wide inlet ammonia velocity (in the range 2−3.4 m/s for these conditions) satisfies both materials stability and breakthrough criteria. For a fixed combustible flow rate, one can vary the ammonia flow rate and tune the power generated over a certain range. To achieve a different power level, one has to vary both the combustible and ammonia flow rates, as elucidated below.

An important observation from Figure 5 is that self-sustained device operation is not feasible at inlet ammonia velocities exceeding 1.56 m/s for a low wall conductivity of $k_s = 3$ W/m/K (solid lines). A possible reason is that the lower heat recirculation via the insulating walls is insufficient to prevent blowout of stable combustion occurring because of the additional heat removal by the endothermic reaction near the reactor inlet. The inset (Figure 5c) shows that the total hydrogen throughput increases with ammonia inlet velocity linearly at first (until ammonia breakthrough), and then it tapers off. For high wall conductivities, a clear maximum occurs for sufficiently high ammonia flow rates because of incomplete ammonia conversion.

Figure 6a shows the maximum wall temperature vs wall thermal conductivity for different inlet velocities of the combustion stream at a constant inlet ammonia velocity. In the shaded region, within which the material stability criterion is satisfied, the wall thermal conductivity has a moderate effect on the wall temperature. Figure 6b shows that the ammonia conversion is slightly dependent on the wall thermal conductivity, with more insulating walls resulting in higher ammonia conversions. Qualitatively similar results are obtained for a fixed flow rate of ammonia and variable combustible flow rate (not shown).

Overall, the wall thermal conductivity moderately affects the preferred operation region primarily because of the materials stability criterion. Low conductivity walls cause hot spot formation and may not allow for effective heat recirculation and thus for sustained operation (Figure 5) for certain (high) propane and ammonia throughputs. More conductive walls alleviate these problems. We return to this point below.

Effect of Device Dimensions. The dimensions of the catalytic microdevice, specifically, the wall thickness (b_w) and the gap sizes of the two channels (d_1 and d_2), affect its performance. As observed in stand-alone microburners,[29] changing the wall thickness has the same effect as that of increasing the wall thermal conductivity. The wall has two roles in the system's thermal response: (i) heat transfer between the two channels and (ii) axial heat recirculation. We define a modified Biot number that gives the ratio of these effects:

$$Bi_a = \frac{h_{gi} l^2}{k_s b_w} = Nu \frac{k_{gi} l^2}{k_s d_i b_w} \quad (10)$$

Since the wall thickness only affects the wall energy balance, the device operation is governed by $k_s b_w$. Consequently, the effect of increasing the wall thickness is exactly the same as increasing the thermal conductivity (studied above) by the same factor (data not shown).

Next, the gap sizes of combustion and ammonia channels were varied individually, from their nominal values of 300 and 200 μm, respectively. For a constant wall thermal conductivity of 15 W/m/K, the modified Biot number also varies with gap size. Two different conditions were considered: (i) the flow rates of the two streams are 1.0 SLPM (combustible mixture) and 0.36 SLPM (ammonia) and (ii) the flow rates are 0.25 and 0.1 SLPM, respectively. These flow rates correspond to the ammonia breakthrough points for $k_s = 15$ W/m/K in Figure 4 and Figure 5, respectively. Note that we kept the flow rates constant, which is the same as keeping a constant Reynolds number and constant power input into the device; the residence times varied with the gap width. Figure 7a shows the maximum temperature (left ordinate, filled symbols) and ammonia conversion (right ordinate, open symbols) versus the ratio of gap width to the nominal gap width of the combustion channel. For both flow rates, the Damköhler number for combustion is greater than 10 when the ratio of gap widths is $(d_1)/(d_1^0) \geq 4$. At the higher flow rate (see solid lines), the system becomes more diffusion limited and propane conversion is incomplete. This results in a drop in temperature, and consequently, a drop in ammonia conversion as well. On the other hand, at the lower flow rate (dashed lines), the system is still diffusion limited. However, the residence time is long enough for complete propane combustion, resulting in higher temperature and, consequently, no ammonia breakthrough.

The same procedure is repeated in Figure 7b for varying the ammonia channel gap size. The ammonia decomposition was reaction-limited for nominal gap size. As a result, increasing the gap size by a factor of 8 did not significantly affect the maximum temperature or the ammonia conversion.

An alternative strategy when varying the gap size is to keep the residence time constant. When the combustion channel gap is doubled, this amounts to doubling the flow rate, resulting in higher temperatures. Likewise, reducing the combustion channel gap leads to lower temperatures and ammonia breakthrough. Similar results were also observed on changing the ammonia gap size, while keeping the ammonia residence time constant.

In summary, proper matching of the flow rates of exothermic and endothermic streams is the most crucial design aspect for coupled cocurrent microreactors (see below). The gap sizes should be made narrow enough so as to avoid diffusion-limited operation. Once in or near the kinetically controlled regime, the device performance is not significantly affected by the gap size, and thus, most submillimeter channels will give excellent performance.

Effect of Inlet Heat Losses. The hot reactor walls can lose heat to the cold feed "reservoir" by convection and radiation from the reactor sidewall. This can be accounted for in the inlet wall boundary condition as

$$\text{At } x = 0 \quad \left\{ k_s \frac{\partial T_s}{\partial x} = h_\infty (T_s - T_{g0}) + \varepsilon \sigma (T_s^4 - T_{g0}^4) \right. \quad (11)$$

This boundary condition replaces the wall boundary condition given in eq T-7. In the above expression, the convective heat loss coefficient was taken as 20 W/m^2/K and the emissivity as 0.7. The primary role of inlet convection and radiation is that it acts as a net heat loss mechanism. Figure 8a shows the maximum wall temperature versus propane inlet velocity at a constant ammonia velocity. The conditions are the same as in Figure 4, except that inlet heat loss is now considered. The shaded region (denoted as R-1) represents the operating region that satisfies the materials stability and ammonia breakthrough criteria. The width of the corresponding operation region of Figure 4a is shown for comparison as the shaded region F-4. With heat losses, the operating region merely moves toward higher propane flow rates.

Likewise, Figure 8b is a plot of the maximum wall temperature versus ammonia inlet velocity for the conditions in Figure 5, now with inlet heat losses. In this case, the operating region moves toward lower ammonia flow rates. Another observation in comparing Figure 8 with Figure 4 or Figure 5 is the qualitative difference observed for various wall conductivities. With insulated sidewalls, the materials stability limit had a weak dependence on the wall thermal conductivity (Figure 4 or Figure 5); with heat losses included, a substantial difference in the material stability limit is observed for the three wall conductivity values. Because of larger heat losses and better heat distribution, the operating region expands slightly for highly conducting walls.

The behavior in the presence of heat losses is as expected: part of the energy released during propane combustion is lost through the inlet. As a result, a greater amount of propane (or equivalently, a lesser amount of ammonia) is required to reach the material stability or the ammonia breakthrough limits. Because of the higher device temperatures at the material stability limit, heat losses affect more this operating line than the ammonia breakthrough limit. Since heat losses from conducting walls are the highest, the material stability limit is affected to a greater extent when having higher conducting walls.

Power Output and Device Efficiency. We now develop attainable regions for operation of the integrated microreactor based on the power that can be generated from the hydrogen produced, assuming 100% efficiency of a downstream device, such as a fuel cell. Figure 9 shows the power output from the device versus the combustible stream inlet flow rate. The power output is used as an indicator of the total hydrogen generated, computed using the lower heating value of hydrogen at 300 K. A two-parameter continuation along the combustible stream and ammonia inlet velocities is performed, keeping track of the maximum wall temperature, ammonia conversion, and hydrogen produced. While these results are shown for $k_s = 300$ W/m/K, results obtained for $k_s = 15$ W/m/K are similar.

As the ammonia flow rate increases at a constant combustible streamflow rate, the power output first increases and eventually decreases; at the same time, the maximum wall temperature decreases (see Figure 5). The loci of operating points, such as the ones shown in Figure 5, versus combustible flow rate are summarized in Figure 9. The dotted line in Figure 9 demarcates the power generated along the materials stability limit. Lower ammonia flow rates result in too high temperatures. The dashed line denotes the power generated at the breakthrough line. Between these two operating lines, temperatures are moderate and conversions are complete. Any further increase in the ammonia flow rate above the breakthrough limit results in incomplete ammonia conversion. On increasing the ammonia flow rate above the breakthrough line, the power output still increases until a certain point (solid line), beyond which the effect of lower ammonia conversion outweighs the increase in

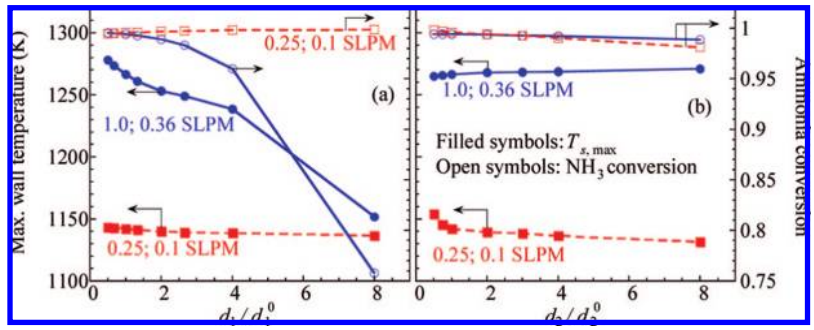

Figure 7. Effect of varying the gap size of (a) the combustion channel and (b) the ammonia channel on the maximum wall temperature (filled symbols) and the ammonia conversion (open symbols). Solid lines represent the case when the flow rates of the combustion and ammonia streams are 1.0 and 0.36 SLPM, respectively, whereas dashed lines 0.25 and 0.1 SLPM, respectively. Both flow rates are close to the ammonia breakthrough limit for the nominal gap sizes (d_1^0 and d_2^0).

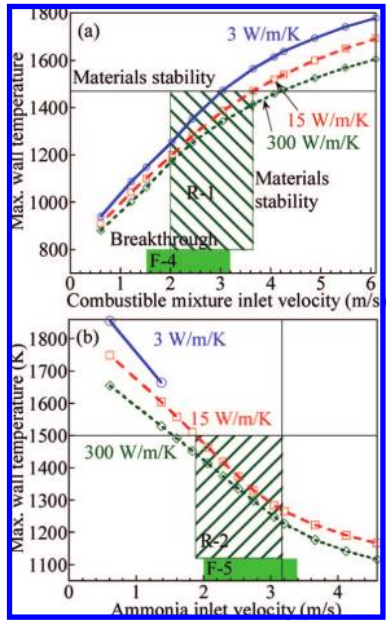

Figure 8. Effect of heat loss through the inlet wall on the maximum wall temperature vs (a) the propane inlet velocity and (b) the ammonia inlet velocity. The shaded (hatched) region in both plots represents the operating region that satisfies both the material stability and the propane breakthrough criteria. The widths of the regions labeled F-4 and F-5 represent operating regions for an adiabatic system; the operating conditions are the same as in Figure 4 and Figure 5, respectively.

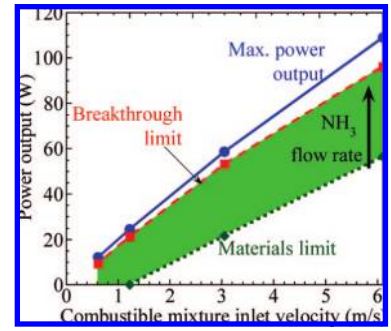

Figure 9. Power output as a function of combustible stream inlet velocity for a wall thermal conductivity of 300 W/m/K. The solid, dashed, and dotted lines represent the maximum power output, the ammonia breakthrough limit, and the materials stability limit, respectively. The power output is computed using the lower heating value of hydrogen generated in the microreactor (i.e., assuming 100% efficiency of a downstream fuel cell). Points are simulation data and lines just connect points.

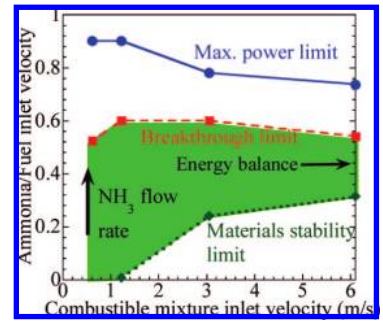

Figure 10. The ratios of ammonia to combustible inlet velocities versus combustible stream inlet velocity for the maximum power, ammonia breakthrough, and materials stability limits of Figure 7 for a wall conductivity of 300 W/m/K. The horizontal arrow indicates the value computed from an overall energy balance at the breakthrough limit. Points are simulation data and lines just connect points.

hydrogen generation owing to the higher ammonia throughput. At much higher ammonia flow rates and low conversions, quenching of the device occurs (now shown).

Figure 10 shows the ratios of inlet velocities of ammonia and combustion streams at the materials stability limit, the ammonia breakthrough limit, and the maximum power lines of Figure 9. A fairly large range of inlet flow velocities exists within which complete conversions occur and device temperatures are reasonable. We have found that in this range of flow rate ratios and in particular close to the breakthrough limit, good overlap of the two reaction zones occurs (see Figure 2C for an example) to minimize temperature gradients. As the flow rates increase (rightmost points of the graph), the temperatures are higher, and ammonia is converted shortly after propane is consumed, that is, one may claim that the overlap of reaction zones is better.

The effect of increasing the ammonia flow rate (along the vertical arrows of Figure 9 or Figure 10) on the device energy efficiency for "once-through" operation is shown in Figure 11 (circles). Herein, efficiency is defined as the ratio of total power output in the form of hydrogen to the total power input as propane and ammonia. As before, the input and output power are computed using the lower heating values of the respective fuels (2045 kJ/mol for propane, 316.8 kJ/mol for ammonia, and 241.8 kJ/mol for hydrogen). Any loss in efficiency arises owing to the heat lost in the form of hot exit gases and unconverted ammonia or propane. The term "once-through" device efficiency indicates that the possibility of recycling or combusting unreacted propane and ammonia, which can improve the overall process efficiency, is not accounted for in this definition. As a

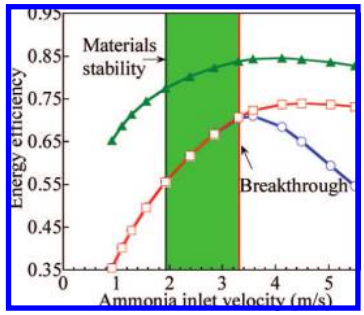

Figure 11. Effect of ammonia inlet velocity on "once-through" device energy efficiency (circles), net energy efficiency (squares), and reformer efficiency (triangles) for a 6.1 m/s propane/air inlet velocity and a 300 W/m/K wall conductivity. The shaded region represents the operating region that satisfies materials stability (left, vertical line) and ammonia breakthrough (right, vertical line) requirements. Points are simulation data and lines just connect points.

result, this is a rather conservative estimate of efficiency. In the literature, different definitions of energy efficiency are used.[37] For example, one could subtract the unutilized ammonia and propane energy content from the denominator. We term this as the net energy efficiency (squares in Figure 11). Another commonly found definition for the reformer (ammonia decomposition in our case) reactor subtracts the sensible heat of the combustion channel (assuming that this is recovered) from the denominator. We term this as the reformer efficiency (triangles in Figure 11).

The shaded region demarcates the operating region compounded from the materials stability and the breakthrough limits. As shown in Figure 11, the maximum "once-through" device efficiency is obtained just beyond the ammonia breakthrough point (along the solid line of Figure 10). In other words, the most efficient microsystem operation occurs close to (but for flow rates above) the breakthrough limit. Still, because of environmental regulations on ammonia and the tolerance limits of PEM fuel cells, significant ammonia breakthrough is not recommended (a separation unit may in fact be needed). The net energy efficiency coincides with the once-through one up to the breakthrough point but is considerably higher in the incomplete conversion regime as recycling of unused reactants is tacitly taken into account. Energy efficiencies approaching ~75% are predicted. The reformer's energy efficiency (triangles) approaches ~85% for the same conditions. In all these energy efficiency calculations, no heat recuperation or heat losses are considered. We project that the once-through device efficiency will increase with heat recuperation but decrease with heat losses. The latter effect will be more important for small scale units. Obviously the optimum efficiency of a system does not solely depend on the microreactor but also on processes downstream of the reactor (e.g., separation, recycling, etc.), which are not examined in this work.

The effect of wall thermal conductivity on the power output of the multifunctional device is shown in Figure 12. The shaded region is the attainable operating region, lying between the materials stability limit and the ammonia breakthrough limit. As in our earlier work,[18] the operating region for the device is much larger for highly conducting walls. For moderate to high wall thermal conductivities, the permissible operating range does not vary much with wall thermal conductivity. This finding is contrary to when heat is supplied via homogeneous propane combustion,[18] wherein highly conducting walls provide the largest range of power output from the multifunctional device, and the operating region shrinks monotonically as the wall conductivity is reduced. For insulating walls (e.g., $k_s = 3$ W/m/K or lower) and high propane/air flow rates (1.0 SLPM or higher), an operating region that satisfies materials stability and ammonia breakthrough limits does not exist. It is clear that moderate to high conductivity walls (~15 W/m/K or higher conductivity) ensure much wider attainable region. Overall, fully catalytic microdevices exhibit a much wider range of operating conditions than their gas combustion-catalytic decomposition counterparts.

Proposed Operational Strategy for Variable Power Output. We believe that the graphical representation of power output (Figure 9 as well as Figures 10− 12) is fairly generic for multifunctional devices up to a maximum combustible flow rate. Related work on steam reforming of methane on Rh actually gives very similar results to support this hypothesis. At higher flow rates (than the ones shown here), additional issues should be considered. For example, either breakthrough of the combustible (residence times lower than ~3 ms) or high temperatures, exceeding the materials stability limit, will eventually occur on increasing flow rates.

The range of power output from a single multifunctional microdevice is on the order of some tens of Watts, and therefore, such small devices (~1 cm × 3 cm × 5 cm = 1.5 cm^3) can be used for portable power generation (electronics). Higher power output (e.g., automotive) can be achieved simply by scaling out, that is, by connecting enough microreactors in parallel. To get an idea of scales, a device of ~1 cm × 3 cm × 5 cm = 15 cm^3 in volume (10 systems, like the one used here, in parallel) can produce up to 1 kW of power. For portable devices, the bulkiest part will be the fuel. Given the higher (by about 2 orders of magnitude) gravimetric energy density of liquid fuels compared to best available Li-based batteries, these devices will be well-suited for decentralized and portable power (e.g., replacing batteries).

Figure 9 indicates that a multifunctional device can be used to generate *variable power* by a suitable choice of both flow rates. Once the breakthrough or maximum power limit have been achieved for a set of conditions, one could "move along a nearly *iso-ratio of flow rates*" curve (see ratios at the breakthrough and maximum power loci in Figure 10) that tracks the breakthrough (or maximum power) curve. We discuss a simple strategy on how to achieve this next.

To estimate the ratio of flow rates at the breakthrough limit, one may use the overall energy balance for the system. On the basis of the energy balances for the gas-phase in the two channels and the solid wall, one has

$$Y^{\mathrm{in}}_{\mathrm{C_3H_8}}\dot{m}_1\Delta H_{\mathrm{comb}} + Y^{\mathrm{in}}_{\mathrm{NH_3}}\dot{m}_2\Delta H_{\mathrm{ref}} + \dot{m}_1 c_{\mathrm{p1}}\left(T_1^{\mathrm{out}} - T_1^{\mathrm{in}}\right) + \dot{m}_2 c_{\mathrm{p2}}\left(T_2^{\mathrm{out}} - T_2^{\mathrm{in}}\right) = 0 \quad (12)$$

Here, Y denotes mass fraction, $\dot{m}$ denotes mass flow rate, the subscripts 1 and 2 refer to the combustion and reforming channel, respectively, and the superscripts "in" and "out" refer to inlet and outlet values. Equation 12 simply states that the net heat release on the wall from the exothermic and endothermic reactions is absorbed as sensible heat in the two channels. In eq 12, the heats of reaction are approximated at 300 K. Assuming complete conversion in both channels at 1300 K, eq 12 gives a ratio of flow velocities of 0.5 (horizontal arrow in Figure 10). The pseudo-2D model for a combustible streamflow rate of 1 SLPM (6.1 m/s) yields a ratio of 0.54 at the breakthrough limit (>99% conversion) at an outlet temperature of 1240 K. This back-of-the-envelop estimate differs by ~7.5% from the prediction of the full code. If the heats of reactions and the exit specific heats are computed at the reactor temper-

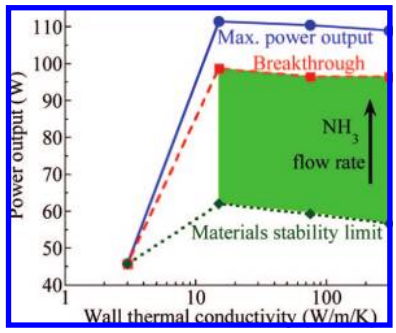

Figure 12. Power output as a function of wall thermal conductivity as the ammonia flow rate increases (from the bottom to the top) for an 6.1 m/s inlet velocity of the combustible mixture. The solid, dashed, and dotted lines represent the maximum power output, the ammonia breakthrough, and the materials stability limits, respectively. At lower wall conductivities (e.g., 3 W/m/K), an operating region that satisfies the materials stability limit does not exist at higher propane/air inlet velocities. Points are simulation data and lines just connect points.

ature, there is practically no error in the estimate (yet one needs the reactor temperature that is unknown without solving the model). Apparently, the better the guess of the outlet temperature at the breakthrough limit at a given combustible streamflow rate, the more accurate the prediction of the ratio of flow rates at the breakthrough point using eq 12. However, even with a poor selection of the outlet temperature (e.g., 1000 K), the prediction of eq 12 remains within a factor 2 from the prediction of the full model (ratio of 0.8 is predicted using eq 12). Thus the overall energy balance with simplifying assumptions is a great estimator of the ratios of flow rates at the breakthrough limit.

The above results suggest a fairly simple operation strategy that can enable variable power output from such a device. The maximum combustible flow rate one can support in a microburner (in the range of milliseconds) delimits the maximum heat input to the system. Higher flow rate results either in blowout or in too high temperatures and should be avoided. A rule of thumb is that the combustible residence time (based on inlet conditions) should be at least a few milliseconds. On the basis of this flow rate, the overall energy balance can then be used to estimate the maximum ammonia flow rate that can be decomposed. The maximum ammonia flow rate in turn determines the maximum power that can be generated (assuming 100% conversion of both streams) per pair of parallel plates. To dial in different power outputs (lower than the maximum one), one could maintain the ratio of flow rates approximately fixed (as determined from the overall energy balance) while reducing both flow rates along the breakthrough line of Figure 7. The lower flow rates are probably determined from the range of the mass flow controllers but could be within an order of magnitude from the maximum.

The above (nearly iso-ratios of flow rates) strategy ensures that one operates close to the breakthrough limit, where complete conversions occur, energy efficiency is close to its maximum, and good overlap of reaction zones is ensured (in Figure 2C, where good overlap of reaction zones is seen, the ratio of inlet velocities is 0.45, close to the estimate using the energy balance discussed above). Moderate (e.g., stainless steal) to high (e.g., silicon carbide) conductivity materials should be preferred to provide the largest attainable operating region. Within this material spectrum, isothermicity is fairly good and slightly less conductive materials have a slight edge regarding conversion. On the other hand, walls are much closer to being isothermal when using more conductive materials.

Conclusions

Thermal coupling of ammonia decomposition on a Ru/alumina catalyst with catalytic propane combustion on Pt/alumina in cocurrent operation mode of a multifunctional parallel plate microreactor was modeled using a pseudo-2D model. The various operating lines delimiting the attainable region were depicted. Stable, self-sustained device operation was found to be feasible at millisecond (or even submillisecond) contact times. This is an important outcome of our work. In comparison to the conventional steam reformer for hydrogen production (residence time of ~1 s), the combination of suitable catalysts and microtechnology enable many-fold reduction in device size and are ideally suited for distributed (e.g., onboard and smaller scale plants) and portable (e.g., electronics) power generation. By comparing to multifunctional systems where the heat is liberated by homogeneous combustion, it is clear (but not necessarily unexpected) that catalytic combustion is the way forward for supplying heat when miniaturizing the system to improve efficiency. Given its high gravimetric hydrogen density and ease of liquefying ammonia, its decomposition in multifunctional microsystems is an excellent platform for CO-free portable and distributed hydrogen production.

A simple operation strategy was proposed that allows one to compute the maximum power output expected from a microdevice. These devices can be used as variable (possibly by as much as 10-fold) power output devices by simply dialing a suitable choice of flow rates. The limits of the power generated are dictated by the range of flow rates allowed by the mass flow controllers and the maximum flow rate of the combustible (a few milliseconds) for self-sustained operation with reasonable temperatures. Heat losses appear to mainly drift the operating regime to higher (combustible) flow rates to compensate for the energy loss. Since the power requirement will most probably vary with time and application, this power tunability of multifunctional devices is an important asset for practical purposes. With this strategy one can operate close to the maximum device energy efficiency (once-through device, ~75%; reformer, ~85%), which is obtained when the reactor is operated slightly in the incomplete conversion regime but close to the breakthrough limit. High conversions and reasonable isothermicity (by having good overlap of reaction zones) are also attained. Decreasing the heat loss to hot products via heat recuperation strategies should enable much higher energy efficiency of a device than the (lower bound) ones reported herein. Moderate to high conductivity walls (~15 W/m/K or higher) are recommended. Finally, when designing microdevices, the gap sizes should be narrow enough to minimize mass transfer limited operation. On this basis, a rough guide is to have a gap width of $\leq 800\ \mu$m for the ammonia channel and a gap width of $\leq 500\ \mu$m for the propane/air channel.

Acknowledgment

This work was supported in part by the NSF (CBET-0729714).

Nomenclature

â = surface area per unit volume (m^2/m^3)
A_0 = pre-exponential factor (s^{-1})
b_w = wall thickness (m)
$\bar{c}_p$ = specific heat of gas (J/kg/K)

c_s = specific heat of solid (J/kg/K)
C = concentration (mol/m^3)
d = gap size (m)
D = diffusivity (m^2/s)
E = activation energy (kcal/mol)
h = coefficient of heat transfer (W/m^2/K)
ΔH = heat of reaction (J/mol)
k = thermal conductivity (W/m/K)
k^{ads} = adsorption rate constant (s^{-1})
k^{des} = desorption rate constant (s^{-1})
k^{rxn} = surface reaction rate constant (s^{-1})
k_{mt} = mass transfer coefficient (m/s)
l = length (m)
$\dot{m}$ = mass flow rate (kg/s)
M = molecular weight (kg/mol)
Nu = Nusselt number
P = pressure (Pa)
R = gas constant (J/mol/K)
r_{gas} = gas-phase reaction rate (mol/m^3/s)
r_{cat} = surface reaction rate (mol/m^2/s)
s = sticking coefficient (−)
Sh = Sherwood number
t = time (s)
T = temperature (K)
u = velocity (m/s)
x = axial coordinate (m)
X = mole fraction
Y = mass fraction

Greek Notations

β = temperature exponent
ε = emissivity
Γ = catalyst site density (mol/m^2)
η = catalyst surface area factor
θ = surface coverage
ν_{kj} = stoichiometric coefficient of species k in reaction j
ρ = density (kg/m^3)
σ = Stefan's constant
τ = time scale (s)
ϕ = equivalence ratio

Subscripts and Superscripts

ads = adsorption
cat = catalyst
des = desorption
endo = endothermic (ammonia) channel
exo = exothermic (combustion) channel
g = gas-phase
k = species index
ref = reference conditions
s = solid wall, surface
0 = inlet conditions
* = vacancies

Literature Cited

(1) NRC. *The Hydrogen Economy: Opportunities, Costs, Barriers and R&D Needs*; The National Academies Press: Washington, DC, 2004.

(2) Brown, L. F. A Comparative Study Of Fuels For On-Board Hydrogen Production For Fuel-Cell-Powered Automobiles. *Int. J. Hydrogen Energy* **2001**, *26*, 381.

(3) Deluchi, M. A. Hydrogen Vehicles - an Evaluation of Fuel-Storage, Performance, Safety, Environmental Impacts, and Cost. *Int. J. Hydrogen Energy* **1989**, *14* (2), 81.

(4) Ganley, J. C.; Seebauer, E. G.; Masel, R. I. Porous Anodic Alumina Microreactors for Production of Hydrogen from Ammonia. *AIChE J.* **2004**, *50* (4), 829.

(5) Choudhary, T. V.; Sivadinarayana, C.; Goodman, D. W. Catalytic Ammonia Decomposition: CO*x*-Free Hydrogen Production for Fuel Cell Applications. *Catal. Lett.* **2001**, *72* (3−4), 197.

(6) Thomas, G.; Parks, G. Potential Roles of Ammonia in a Hydrogen Economy. Technical Report; U.S. Department of Energy, 2006.

(7) Pyrz, W.; Vijay, R.; Binz, J.; Lauterbach, J.; Buttrey, D. J. Characterization of K-Promoted Ru Catalysts for Ammonia Decomposition Discovered Using High-Throughput Experimentation. Top. Catal. In press.

(8) Deshmukh, S. R.; Mhadeshwar, A. B.; Vlachos, D. G. Microreactor Modeling for Hydrogen Production from Ammonia Decomposition on Ruthenium. *Ind. Eng. Chem. Res.* **2004**, *43*, 2986.

(9) Ferreira-Aparicio, P.; Benito, M. J.; Sanz, J. L. New Trends in Reforming Technologies: From Hydrogen Industrial Plants to Multifuel Microreformers. *Catal. Rev.—Sci. Eng.* **2005**, *47* (4), 491.

(10) Agar, D. W.; Ruppel, W. Multifunctional Reactors for Heterogeneous Catalysis. *Chem. Ing. Tech.* **1988**, *60* (10), 731.

(11) Bolk, J. W.; Siccama, N. B.; Westerterp, K. R. Flammability Limits in Flowing Ethene-Air-Nitrogen Mixtures: An Experimental Study. *Chem. Eng. Sci.* **1996**, *51* (10), 2231.

(12) Kolios, G.; Glokler, B.; Gritsch, A.; Morillo, A.; Eigenberger, G. Heat-Integrated Reactor Concepts for Hydrogen Production by Methane Steam Reforming. *Fuel Cells* **2005**, *5*, 52.

(13) Matros, Y. S.; Bunimovich, G. A. Reverse-Flow Operation in Fixed Bed Catalytic Reactors. *Catal. Rev.—Sci. Eng.* **1996**, *38* (1), 1.

(14) Deluga, G. A.; Salge, J. R.; Schmidt, L. D.; Verykios, X. E. Renewable Hydrogen from Ethanol by Autothermal Reforming. *Science* **2004**, *303* (5660), 993.

(15) Hickman, D. A.; Schmidt, L. D. Production of Synthesis Gas by Direct Catalytic Oxidation of Methane. *Science* **1993**, *259*, 343.

(16) Zanfir, M.; Gavriilidis, A. Catalytic Combustion Assisted Methane Steam Reforming in a Catalytic Plate Reactor. *Chem. Eng. Sci.* **2003**, *58* (17), 3947.

(17) Deshmukh, S. R.; Vlachos, D. G. CFD Simulations of Coupled, Countercurrent Combustor/Reformer Microdevices for Hydrogen Production. *Ind. Eng. Chem. Res.* **2005**, *44* (14), 4982.

(18) Deshmukh, S. R.; Vlachos, D. G. Effect of Flow Configuration on the Operation of Coupled Combustor/Reformer Microdevices for Hydrogen Production. *Chem. Eng. Sci.* **2005**, *60* (21), 5718.

(19) Gosiewski, K. Mathematical Simulations of Reactors for Catalytic Conversion of Methane to Syngas with Forced Concentration Cycling. *Chem. Eng. Proc.* **2000**, *39* (5), 459.

(20) Kulkarni, M. S.; Dudukovic, M. P. A Bidirectional Fixed-Bed Reactor for Coupling of Exothermic and Endothermic Reactions. *AIChE J.* **1996**, *42* (10), 2897.

(21) Blanks, R. F.; Wittrig, T. S.; Peterson, D. A. Bidirectional Adiabatic Synthesis Gas Generator. *Chem. Eng. Sci.* **1990**, *45* (8), 2407.

(22) DeGroote, A. M.; Froment, G. F.; Kobylinski, T. Synthesis Gas Production from Natural Gas in a Fixed Bed Reactor with Reversed Flow. *Can. J. Chem. Eng.* **1996**, *74* (5), 735.

(23) Gosiewski, K.; Bartmann, U.; Moszczynski, M.; Mleczko, L. Effect of the Intraparticle Mass Transport Limitations on Temperature Profiles and Catalytic Performance of the Reverse-Flow Reactor for the Partial Oxidation of Methane to Synthesis Gas. *Chem. Eng. Sci.* **1999**, *54* (20), 4589.

(24) Kaisare, N. S.; Lee, J. H.; Fedorov, A. G. Hydrogen Generation in a Reverse-Flow Microreactor: 1. Model Formulation and Scaling. *AIChE J.* **2005**, *51* (8), 2254.

(25) Annaland, M. V.; Scholts, H. A. R.; Kuipers, J. A. M.; van Swaaij, W. P. M. A Novel Reverse Flow Reactor Coupling Endothermic and Exothermic Reactions. Part 1: Comparison of Reactor Configurations for Irreversible Endothermic Reactions. *Chem. Eng. Sci.* **2002**, *57* (5), 833.

(26) Fissore, D.; Barresi, A. A.; Baldi, G. Synthesis Gas Production in a Forced Unsteady-State Reactor Network. *Ind. Eng. Chem. Res.* **2003**, *42* (12), 2489.

(27) Norton, D. G.; Deshmukh, S. R.; Wetzel, E. D.; Vlachos, D. G. Downsizing Chemical Processes for Portable Hydrogen Production. In *Microreactor Technology and Process Intensification*; Wang, Y., Holladay, J. D., Eds.; ACS: New York, 2005; p 179.

(28) Vlachos, D. G., *Microreaction Engineering: Processes, Detailed Design and Modeling*; Barton, P. I., Mitsos, A., Eds.; Wiley-VCH: New York, 2008.

(29) Kaisare, N. S.; Deshmukh, S. R.; Vlachos, D. G. Stability and Performance of Catalytic Microreactors: Simulations of Propane Catalytic Combustion on Pt. *Chem. Eng. Sci.* **2008**, *63*, 1098.

(30) Kee, R. J.; Rupley, F. M.; Miller, J. A., *The CHEMKIN Thermodynamic Database*. Sandia National Laboratories ReportSAND87-8215B; Sandia National Laboratories: New Mexico, 1991.

(31) Kee, R. J.; Dixon-Lewis, G.; Warnatz, J.; Coltrin, M. E.; Miller, J. A., *A FORTRAN computer Code Package for the Evaluation of Gas Phase Multicomponent Transport Properties*. Sandia National Laboratories Report SAND86−8246; Sandia National Laboratories: New Mexico, 1990.

(32) Kaisare, N.; Stefanidis, G. D.; Vlachos, D. G. Transport Phenomena in Microscale Reacting Flows. In *Handbook of Microprocess Engineering: Fundamentals, Operations, and Catalysts*; Renken, A., Wang, Y., Eds.: Wiley-VCH: Berlin, 2008.

(33) Petzold, L. R. Automatic Selection of Methods for Solving Stiff and Nonstiff Systems of Ordinary Differential Equations. *Siam J. Scien. Stat. Comput.* **1983**, *4*, 136.

(34) Deshmukh, S.; Vlachos, D. G. A Reduced Mechanism for Methane and one-step Rate Expressions for Fuel-Lean Catalytic Combustion of Small Alkanes on Noble Metals. *Combust. Flame* **2007**, *149* (4), 366.

(35) Mhadeshwar, A. B.; Vlachos, D. G. Is the Water−Gas Shift Reaction on Pt Simple? Computer-aided Microkinetic Model Reduction, Lumped Rate Expression, and Rate-Determining Step. *Catal. Today* **2005**, *105* (1), 162.

(36) Deshmukh, S. R. Design Principles for Multifunctional Microchemical Systems: Applications to Hydrogen Production. Ph.D. Thesis. University of Delaware, Newark, DE, 2006.

(37) Lutz, A. E.; Bradshaw, R. W.; Keller, J. O.; Witmer, D. Thermodynamic Analysis of Hydrogen Production by Steam Reforming. *Int. J. Hydrogen Energy* **2003**, *28*, 159.

Received for review March 10, 2008
Revised manuscript received October 16, 2008
Accepted December 4, 2008

IE800392Z